2nd International Engineering Conference (IEC 2017)
Federal University of Technology, Minna, Nigeria

Synthesis and Characterization of TiO_2 Nanorod Supported on Stainless Steel Mesh Prepared Via Sol-Gel Method

*Tijani, J.O[1,4], Mustapha, S.I.[2], Bankole, M.T.[1,4], & Amigun, A.T[3]
[1]Department of Chemistry, Federal University of Technology, PMB 65, Bosso Campus, Minna, Niger State, Nigeria
[2]Department of Chemical Engineering, University of Ilorin, PMB 1515, Ilorin, Kwara State, Nigeria
[3]Department of Chemical and Geological Sciences, Al-Hikmah University, Ilorin, Kwara State, Nigeria
[4]Nanotechnology Research Group, Centre for Genetic Engineering and Biotechnology (CGEB), Federal University of Technology, P.M.B 65, Bosso, Minna, Niger State, Nigeria
*Corresponding author email: jimohtijani@futminna.edu.ng, +2348057344464

ABSTRACT
Semiconductor metal oxide such as TiO_2 has received significant attention in the field of material science owing to its low cost, stability, environmental friendliness and excellent photocatalytic activity. However, fast electron-hole recombination rate, high band gap, post-separation and recovery of the used TiO_2 photocatalysts from wastewater after treatment limited its full scale industrial applications. In the light of this background, the present study investigated the synthesis of TiO_2 nanorods supported on stainless steel mesh using a sol-gel solution of Polyvinylpyrrolidone (PVP), ethanol and titanium tetrachloride ($TiCl_4$). The influence of pyrolysis temperature on the particles size, morphologies, microstructures and surface areas on the prepared supported catalyst were investigated. The as-synthesised nanorods were characterized by High Resolution Scanning Electron Microscope (HRSEM), High Resolution Transmission Electron Microscope (HRTEM), Energy Diffraction Spectroscopy (EDS), X-ray Diffraction (XRD), Brunauer-Emmett-Teller (BET) surface area, and X-ray photoelectron spectroscopy (XPS) analysis. The HRSEM and HRTEM analysis confirmed the formation of densely grown, well defined and uniformly aligned nanorod covered the whole surface of stainless steel mesh. The XRD analysis demonstrated the formation of pure tetragonal anatase phase of TiO_2 irrespective of pyrolysis temperature and no rutile or brookite phase were detected. The average crystalline size of TiO_2 nanorod decreased from 45 nm to 28 nm as the temperature increases from 300°C to 400 °C at constant holding time of 2 hrs. The specific surface area of the supported as-synthesised TiO_2 nanorods was in the order of prepared at 400 °C (81 m^2/g) > 350 °C (77 m^2/g) > 300 °C (62 m^2/g). The XPS analysis revealed the Ti in the prepared TiO_2 is in +4 electronic state. This study has demonstrated that PVP/ethanol/$TiCl_4$ offers a facile, robust sol-gel related route for preparing supported TiO_2 nanorod.

Keywords: *Sol-gel method, TiO_2 nanorod, synthesis, stainless steel mesh*

1 INTRODUCTION

In the last couple of years, semiconductor metal oxides such as ZnO, TiO_2, WO_3, Fe_2O_3, ZnS, CdS, GaP, $ZrTiO_4$, and SiO_2 have been utilized for different purposes in the field of the photocatalytic technology. Among the aforementioned heterogeneous metal oxides, TiO_2 photocatalysts has received considerable attention in the field of material science due to its low cost, photochemical stability, environmental friendliness and exceptional photocatalytic behaviour (Liu et al., 2016; Shinde et al., 2015; Zhao et al., 2017). Titanium (IV) oxide can be found in the natural form of titanic anhydride or titanic acid anhydride and exists in three major phases namely rutile, anatase and brookite (Álvarez et al., 2010; Gharakhlou and Sarvi, 2017). And among the phases, anatase remains the most preferred owing to its photocatalytic and photochemical stability. Titanium precursor such as $TiCl_4$ or titanium alkoxides are mostly used in the preparation of anatase TiO_2.

However, high electron-hole recombination rate from valence band to conduction band contributed to the low photosensitivity and photocatalytic efficiency of TiO_2 (Bestetti et al., 2010; Gaya and Abdullah, 2008; Tijani et al., 2017). Also, high capital and running cost associated with the post-separation and recovery of the used TiO_2 photocatalysts from wastewater after treatment limits its full scale industrial applications (Hintsho et al., 2014; Jiang et al., 2017). In view of the highlighted shortcomings, different approaches have been adopted to overcome the challenges. One of such strategies is the doping or immobilisation of TiO_2 nanoparticle with metals and non-metals impurities, semiconductor coupling or sometimes fluorination process (Tijani et al., 2017). Doping creates a defect level within the band gap causing reduction in the electron excitation of TiO_2 and possibly extends the absorption threshold to the visible region and enhanced the photocatalytic activity (Kuriechen and Murugesan, 2013; Lee et al., 2015; Nunes et al., 2017). Supported or unsupported Nano TiO_2 materials in the form of powder, crystals, rods, or thin-films have been prepared via different methods namely; electrochemical, magnetic sputtering, photo deposition, sulfate process, chloride process, solvo-thermal, electron beam evaporation, precipitation, hydrothermal, chemical vapour deposition, thermal evaporation, wet impregnation dip coating, and sol–gel process (Carlucci et al., 2014; Chong

et al., 2010; Jiang et al., 2017). Among the aforementioned techniques, sol-gel technique appeared most suitable due to ease of manipulation of synthesis conditions resulting to the formation of nanoparticles with good homogeneity and precise phase structure (Monreal et al., 2009; Nainani et al., 2012; Wahyuningsih, et al., 2017).

Furthermore, researchers have developed TiO_2 nanomaterials on different fixed supports such as zeolite, clay, activated carbon, glass fiber, quartz, stainless steel mesh amongst others in order to solve the post-filteration of TiO_2 particles after treatment (Omri et al., 2015). Till date, efforts are still ongoing towards finding a suitable and stable substrate to support TiO_2-based photocatalyst and only very few reports exist on the synthesis of supported TiO_2 nanorods (Zhang et al., 2017). For instance, Lia et al., (2009) prepared crystalline TiO_2 nanorod array on the pre-treated glass substrate via hydrothermal route and found that the well-aligned single crystal of TiO_2 grown on pre-treated glass substrate exist as a rutile polymorph with an average diameter and length of approximately 21 and 400 nm, respectively. Mahendiran et al., (2014) prepared unsupported TiO_2 nanorods via a novel direct sol filling and heating sol-gel template method involving titanium (IV) isopropoxide as a precursor. The authors found that the as-prepared TiO_2 nanorod exhibited pure anatase polymorph with an average size of 10 nm and 99% of Ti existed in +4 oxidation state. Shinde et al., (2015) reported the hydrothermal synthesis of TiO_2 nanorods on Transparent Conducting Oxide (TCO) and found that the deposited TiO_2 nanorods were purely rutile phase with tetragonal crystal structure.

In this present work, stainless steel mesh supported TiO_2 nanorods were synthesized using sol-gel solution comprises Polyvinylpyrrolidone (PVP), ethanol and titanium tetrachloride ($TiCl_4$). The influence of pyrolysis temperature on the size and shape of the nanorods were investigated. The prepared supported TiO_2 nanorods were characterised for their morphologies, microstructures, elemental composition, mineralogical phases, surface areas, and surface chemical states using High Resolution Scanning Electron Microscope (HRSEM), High Resolution Transmission Electron Microscope (HRTEM), Energy dispersive X-ray spectroscopy (EDS), X-ray diffraction (XRD), Brunauer–Emmett–Teller (BET) measurements, and X-ray photoelectron spectroscopy (XPS).

2 METHODOLOGY

2.1. MATERIALS

Titanium (IV) chloride with (0.09 M in 20% HCl) and Polyvinylpyrrolidone (500 g) powder were obtained from Sigma Aldrich. While ethanol was supplied by B & M Scientific. The chemicals were of analytical grade and used without any further purification.

2.2 SYNTHESIS OF TIO_2 NANOROD SUPPORTED ON STAINLESS STEEL MESH

Twenty (20) gram Polyvinylpyrrolidone (PVP) was added to 40 mL ethanol in a beaker and stirred on a hot plate until the PVP completely dissolved and a yellowish transparent gel was obtained. 10 mL titanium (IV) chloride solution was slowly added to 20 mL solution containing PVP and ethanol. The mixture was sealed in a bottle and then stirred on a magnetic stirrer at room temperature (25 °C) for 3 hrs. At the end of 3 hrs stirring, a slightly transparent PVP/$TiCl_4$ viscous solution was obtained. This step was conducted in a ventilated fume hood. During the addition of 10 mL of 0.09 M $TiCl_4$, the transparent solution rapidly became a brownish yellow in colour. The addition of 6 mL of 0.09 M $TiCl_4$ was accompanied by the release of white fumes of hydrochloric acid, and the stirring was continued for 15 min until the white fumes disappeared. The formed viscous solution was continually stirred until the white fumes disappeared.

Before manual coating of the stainless steel mesh with sol-gel, a 4 × 4 cm stainless steel mesh was rinsed with acetone, ethanol and water, and then dried in an oven at 90 °C for 5 min in order to remove organic and inorganic contaminants. The cleaned stainless steel mesh was weighed and coated manually with the prepared sol-gel formulation of PVP/$TiCl_4$. The sol-gel solution was coated on 4 × 4 cm stainless steel mesh using the dip-coating method with a drawing speed of 5.0 cm/min. This procedure was repeated three times and thereafter the coated mesh was air dried and later pyrolysed in the furnace at different temperature 300 °C, 350 °C and 400 °C. A heating rate of 50 °C/min and holding time of 2 hrs was adopted. The procedure also included a flow of nitrogen gas through the inner tube at 20 mL/min in order to create an inert environment and to prevent side reactions such as hydrolysis. The synthesized supported TiO_2 nanorods prepared at different temperature 300 °C, 350 °C and 400 °C for 2 hrs holding time was coded JT1, JT2 and JT3.

2.3. CHARACTERIZATION OF SUPPORTED TIO_2 NANOROD

Philips X-pert pro MPD X-ray diffractometer (XRD) Cu-K radiation at 40 kV and 40 mA was used to determine the phase composition and estimation of the crystal size of the synthesised catalysts. The X-ray patterns were scanned in the 2θ range from 200-800 with a step 0.050, counting time 1s/step. The crystalline size was calculated from the peak full-width at half maximum with corrections for instrument line broadening by using the Scherer equation. $D = k\lambda/(\beta \cos\theta)$, $K = 0{\cdot}89$, $\lambda = 0{\cdot}1541$ nm, θ is the half-diffraction angle, β the half-peak width, D the diameter of crystalline particle. HRSEM equipped with EDS was used to determine the particle morphology and elemental composition of the synthesised catalysts. Microstructures and particle distribution patterns were

analyzed by a Zeiss Auriga High resolution transmission electron microscope (HRTEM). Approximately 0.02 g of the synthesised products was suspended in 10 mL methanol and thereafter subjected to ultra-sonication until complete dispersion was achieved. One or two drops of the slurry was dropped onto a holey carbon grid with the aid of a micropipette and subsequently dried via exposure to photo light. For BET N_2 adsorption, about 100 mg of the dry powder sample in a sample tube, was first degassed at 90°C for 4 hours to remove residual water and other volatile components that were likely to block the pores. The BET surface area and average pore volume distributions were obtained from the plot of volume adsorbed (cm3/g STP) versus relative pressure. The N_2 adsorption-desorption isotherms were collected at -196° C using Micromeritics ASAP 2020 Accelerated Surface Area and Porosimetry analyser. A XPS PHI 5400 equipped with hemispherical sector analyser operated using non-monochromated Al Kα x-rays with energy 1486.6 eV, at 300 W and 15 kV was used to examine the surface composition of the material. The energy scale was calibrated using the Au 4f7/2 at 83.95 eV and the linearity of the scan was adjusted to measure the Cu $2p_{3/2}$ at a position of 932.63 eV. Surveys were scanned (2.5 eV/s) with pass energy of 178 eV and detailed spectra were collected with pass energy of 44 eV and scan rate of 0.625 eV/s. The photoelectron take-off angle for all measurements was 45°. All spectra obtained were energy corrected using the aliphatic adventitious hydrocarbon C (1s) peak at 284.8 eV. The XPS Peak 4.1 software was used for data analysis and fits.

3 RESULTS AND DISCUSSION

High resolution scanning electron microscopy (HRSEM) was used to examine the morphology of the prepared supported TiO_2 nanorods. The HRSEM micrographs of the titania nanorods at different temperatures (300 – 400 °C) for 2 hrs holding time are depicted in Fig. 1. As shown in Fig. 1(a), there was no formation of nanorods on the stainless steel mesh, when the pyrolysed temperature was 300 °C (Fig 1 (b)), instead agglomerated irregular nanocrystals and nanorods that stick to the stainless steel mesh were observed. This implies that the polymer precursor (PVP) is not stable at temperature beyond 200 °C, thus initiation of crystallization of the $TiCl_4$ precursor into TiO_2 nanorods occurred. The length of the nanocrystals and nanorods according to imageJ software were found to be 10 nm and 16.8 nm respectively. As the pyrolysed temperature increases to 350 °C (Fig. 1 (c)) uniformly distributed, well aligned, densely agglomerated tetragonal bunches-like morphology were observed. The length of the nanorods increased to 35 nm at 350 °C for 2 hrs holding time and a complete disappearance of the nanocrystals was observed. This suggests thermal conversion of the PAN into carbonaceous species during the heating period. With further increase in temperature to 400 °C, short, homogeneous, completely grown, regularly aligned and less aggregated nanorods resembling rice grain were observed. With increasing the pyrolysis temperature, the length of the nanorods slightly reduced to 26 nm. This was an evidence of a fast nucleation process responsible for the formation of densely grown, well defined and uniformly aligned nanorod. The reduction in the size of the nanorods is an indication that the as-synthesised supported TiO_2 nanorod flowers may have a large surface area and exhibit high photocatalytic activity under the incident photons (Omri et al., 2015). It is worthwhile to note, that PAN and its decomposition products acts as an adhesive that stick the TiO_2 nanorods together onto the stainless steel mesh. It is evident that the morphological evolution that is the shape and size of the nanorod is strongly a temperature dependent phenomenon.

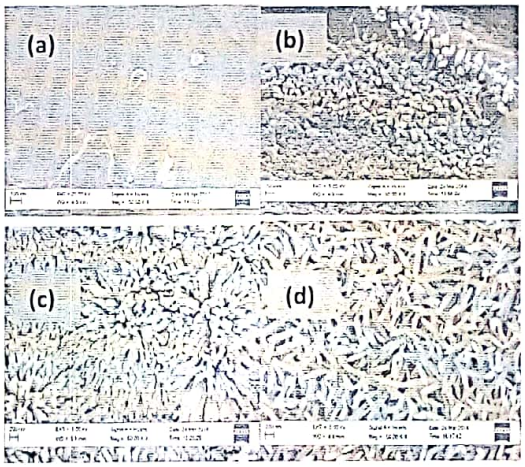

Fig. 1: HRSEM micrographs of (a) stainless steel mesh alone (b) titania nanorods prepared at 300 °C (c) titania nanorods supported prepared at 350 °C (d) titania nanorods supported on stainless steel mesh deposited at 400 °C for 2 hrs

HRTEM ANALYSIS

HRTEM was utilized to further examine the detailed microstructures of the supported TiO_2 nanorods prepared by pyrolysis at 300°, 350°, or 400° C for 2 hrs. The HRTEM micrographs of the supported TiO_2 nanorods pyrolyzed at 300 °C, 350 °C or 400 °C in N_2 atmosphere at 20 mL/min for 2 hrs is represented in Fig. 2. Fig. 2 shows the HRTEM images of supported TiO_2 nanorods prepared by pyrolyzed in N_2 atmosphere at 300 °C for 2 hrs. In Fig. 2 (a), a mixture of nanocrystals and nanorods were formed, which means that some of the $TiCl_4$ precursor was still embedded in the gradually decomposing PVP polymer. With increase in temperature to 350 °C for 2 hr holding time, the initially observed mixed nanocrystals and nanorods completely transformed to a full, thick,

smooth and orderly arranged nanorods (Liu et al., 2016). This clearly shows complete decomposition of PVP and non-entrapment of $TiCl_4$ precursor. Furthermore, the length of the nanorod was determined using imageJ and found to be in the range of 35 to 40 nm. When the temperature was increased to 400 °C hr (Fig.2 c), a well resolved, thin and highly crystalline TiO_2 nanorods was homogeneously deposited on the stainless steel mesh.

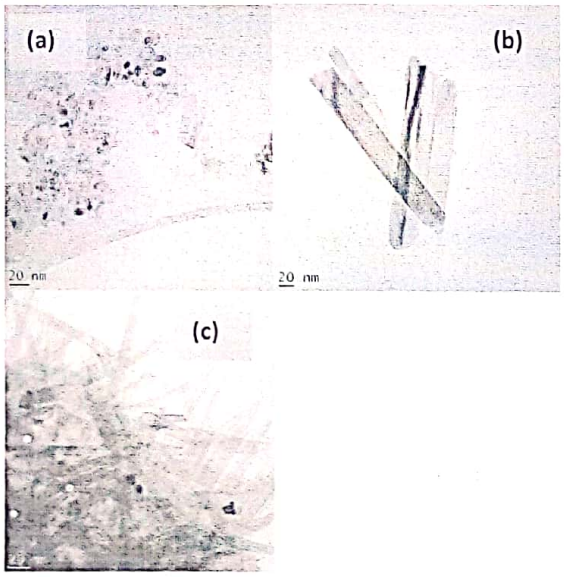

Fig. 2: HRTEM micrographs of (a) titania nanorods supported on stainless steel mesh deposited at 300 °C (b) titania nanorods supported on stainless steel mesh deposited at 350 °C (c) titania nanorods supported on stainless steel mesh deposited 400 °C for 2 hrs

EDS ANALYSIS

An elemental composition analysis of the stainless steel mesh and that of the as-synthesised supported TiO_2 nanorods were determined using EDS. Fig. 3 (a) and (b) show the EDS spectra of stainless steel mesh alone and supported TiO_2 nanorods. The EDS spectrum of stainless steel mesh recorded in the binding energy region of 0–20 keV and the following individual elements C, Cr, Fe, Ni, Si, Mo were detected in different proportion.

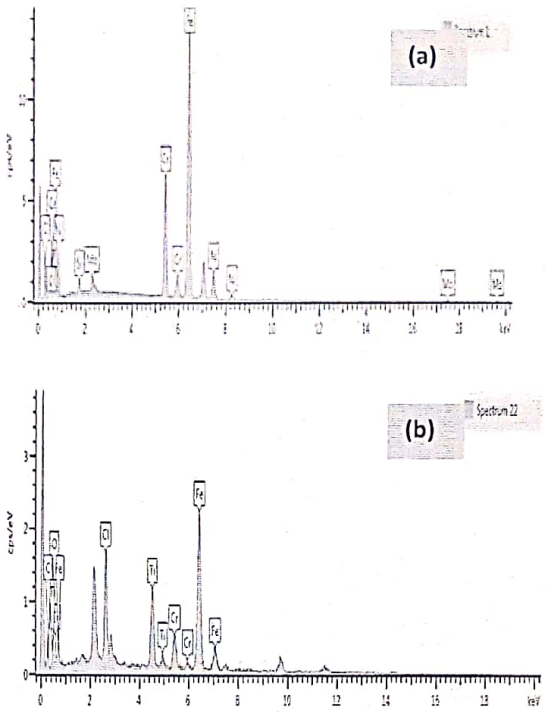

Fig. 3: EDS spectrum of (a) ordinary stainless steel mesh (b) TiO_2 nanorods supported on stainless steel mesh

However, in Fig. 3 (b), two prominent signals different from Fig 3 (a) were noticed in the binding energy region of 4.508 and 0.525 keV respectively, which corresponds to Ti and O were identified. This means that the as-synthesised catalyst consist Ti and O with a near atomic ratio of 1:2 which is closely agrees with the stoichiometry of TiO_2. The atomic percentages of Ti and O in the prepared samples are approximately 36.21% and 22.80% respectively. The elements such as Fe and Cr originated from the stainless steel mesh while the residual chlorine is from the titanium precursor ($TiCl_4$).

XRD ANALYSIS

XRD analysis was done to investigate crystallite size and crystal structure of the TiO_2 nanorods. Fig. 4 reveals the influence of pyrolysis temperature on the crystalline nature of the as-synthesised materials. XRD pattern in Fig. 4 (a) exhibited weak diffraction peaks at the 2 thetha value of 58.2, 59.2 and 66.1, which correspond to Fe, Cr and Si respectively. Besides these elements, it can be seen from the XRD patterns especially Fig. 4 (b-d) the presence of the following strong broad diffraction peaks at 25.55°, 38.3°, 47.5°, 53.60°, 63.2°, 69.7°, and 75.2° irrespective of the pyrolysed temperature. These diffraction peaks indicate the presence of following crystal planes (101), (004), (200), (211), (204), (220), and (215).

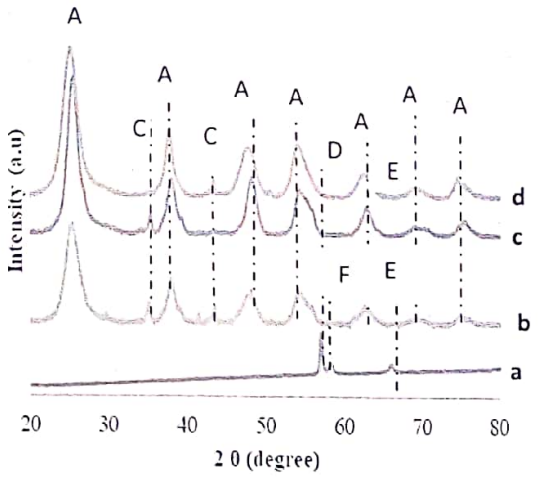

Fig. 4: XRD pattern of the catalysts: (a) stainless steel mesh alone (b) (300 °C for 2 hrs) (c) (350 °C for 2 hrs) (d) (400 °C for 2 hrs) at constant heating rate of 50 °C/min A=anatase, C=carbon, D=Fe, F=Cr E=Si

All diffraction peaks closely agree with the standard (JCPDS: No 21-1272). The strong peak clearly seen from Fig. 4 (b-d), confirmed the formation of highly crystalline TiO2 products. For each temperature, the XRD patterns showed the formation of pure the tetragonal crystal anatase polymorph of TiO_2 nanorods and no peaks correspond to rutile or brookite phases at each temperature were noticed. Other diffraction peaks observed in Fig 4 (b-c) at 2 thetha value of 35.4° (002), 41.2° (111) and 45.4° (100) are characteristics peaks of a typical carbon species derived from PVP. Carrenõ et al., (2008) shown that during the pyrolysis reaction, polymer precursor often decomposed to residual carbon and possible replacement of oxygen in TiO_2 by carbonaceous materials from PVP precursor and Ti-O-C bond possibly formed (see Fig.8). It was observed that as the pyrolysis temperature increases the carbon peak disappeared, an indication of partial or complete decomposition of PVP and no further encapsulation or entrapment of the nanorods within the polymer precursor chain. This further suggests that as the temperature increases, there was a simultaneous pyrolysis of PVP followed by oxidation of $TiCl_4$ precursor into TiO_2 nanorods. The average size of the nanorods were determined using using the Debye-Scherrer equation shown in equation 1, where the 2 thetha value of the intense anatase peak (101) in the synthesized TiO_2 nanorods was selected.

$$d = \frac{k\lambda}{\beta \cos\theta}$$

.....(1)

where d in equation 1 represents the crystallite size in nanometer, K = 0.94, λ is the wavelength and equal to 0.1541 nm, 0 is the half-diffraction angle, β is the full width at half-maximum in radian of 2 0 value (25.55°). According to equation 1, the average crystalline size of TiO_2 nanorod decreased from 45 nm to 28 nm as the temperature increases from 300°C to 400 °C at constant holding time of 2 hrs. The slight broad nature of the diffraction peaks at 2 thetha value of 25.3° may be responsible small size of the nanorods.

BET ANALYSIS

The N_2 adsorption–desorption isotherms of the TiO_2 nanorods supported on stainless steel mesh pyrolysed in the furnace at 300 °C, 350 °C and 400 °C for 2 hrs are shown in Figure 5.

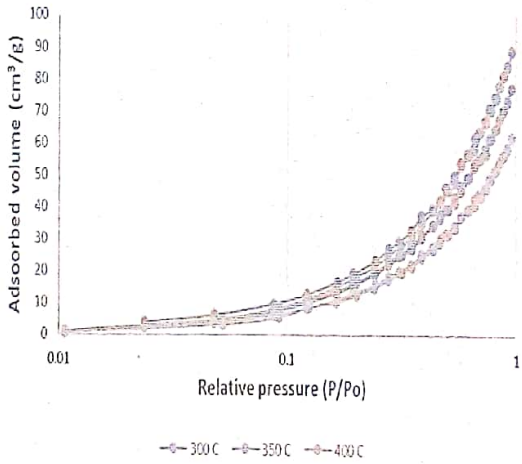

Fig.5: BET surface area of the prepared supported TiO_2 nanorods at different temperature

The specific surface areas and pore volumes determined using Micrometrics ASAP 2020 surface area and Porosity Analyzer are shown in Table 1. According to Table 1, the BET specific surface areas of the as-prepared supported TiO2 nanorods at 300 °C, 350 °C and 400 °C pyrolysis temperature and constant holding time of 2 hrs are 62, 77 and 81 m^2/g. It is evident from Table 1 that, as the temperature increases the BET surface area also increases, which is attributable to the thermal decomposition of PVP into carbonaceous species and incorporation of such carbon onto the lattice crystals of the supported titania rods.

TABLE 1: SPECIFIC SURFACE AREA AND PORE VOLUME OF AS-SYNTHESISED SUPPORTED TIO_2 NANORODS COMPARED TO THE COMMERCIAL TIO_2 POWDER (DEGUSSA P25)

Samples	BET surface area (m^2/g)	Pore volume (cm^3/g)
P25 (commercial TiO_2)	56	0.64
300°C for 2 hr	62	1.12
350°C for 2 hr	77	1.21
400°C for 2 hr	81	1.35

It was also noticed that the surface area of the as-synthesised TiO_2 nanorods is greater than that of commercial TiO_2 nanoparticles. The possible reason for the increased specific surface area might be attributed to the pyrolysis temperature and the immobilisation effect of carbonaceous species from PVP, which perhaps lead to substitution of the oxygen in TiO_2 with carbon. According to the IUPAC classification, the as-synthesised supported TiO_2 nanorod exhibited type IV-isotherm and H_2 hysteresis respectively irrespective of the pyrolysis temperature. This is an indication that the synthesized samples are mesoporous in nature as evident in the sloping adsorption branch of loop and small pore volume. In addition, the presence of a relatively sharp steep desorption branch observed at high relative pressure (P/P_0) range also suggest the formation of mesoporous material with particles size in the range of 2 -50 nm.

XPS ANALYSIS

The XPS analysis was done to identify the possible chemical state or the surface valence states of elements present in the supported TiO_2 nanorods. Fig. 6 represents the High resolution XPS survey of the supported TiO_2 nanorods prepared at 400 °C for 2 hrs.

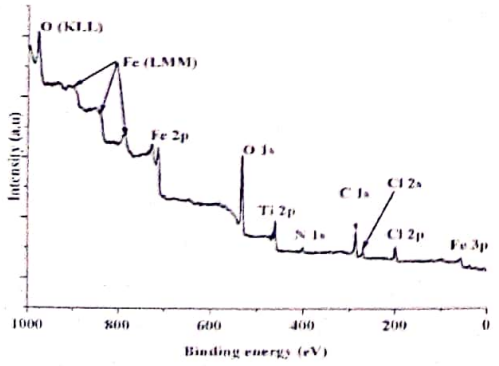

Fig. 6: General XPS survey of supported TiO_2 nanorods pyrolysed at 400 °C for 2 hrs

The general survey of the supported TiO_2 nanorods pyrolysed at 400 °C for 2 hrs revealed the presence of the following elements: Fe, O, Ti, N, C, and Cl. The Fe originated from the stainless steel mesh while Cl and N are from titanium and polymer precursor respectively. The binding energy regions of 459.12 and 530.6 eV correspond to Ti 2p and O 1s respectively. Furthermore, the XPS survey shown in Fig. 8 depict the Ti 2p and possessed two peaks in the binding energy region of 459.2 and 465.7 eV.

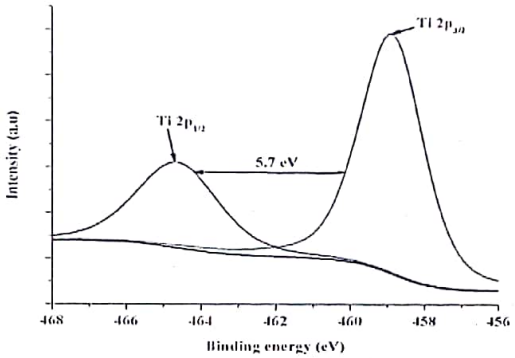

Fig. 7: XPS survey of Ti 2p envelop in TiO_2 nanorods

Also in Fig. 7, it can be noticed that there is an existence of one broad, sharp and narrow peaks at the binding region of 459.3 and 465 eV. This implies that the Ti in TiO_2 nanorods exist in +4 oxidation state. The sharp peak in the Ti 2p orbital connote Ti $2p_{3/2}$ while the broad peak represents Ti $2p_{1/2}$. The presence of these two orbitals mean that Ti occurred in one chemical state. Moreso, the differences between the binding energies values of Ti $2p_{3/2}$ and Ti $2p_{1/2}$ was 5.7 eV, which further buttress the fact that Ti existed in +4 chemical state in the as-synthesised TiO_2 nanorods. The binding energies for Ti and O obtained in this study agree with the literature value reported for TiO_2 nanorods (Lia et al., 2009; Mahendiran et al., 2014; Shinde et al., 2015)

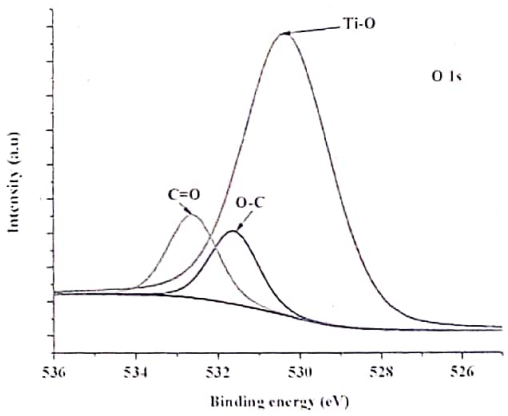

Fig. 8: The XPS spectrum of O 1s enveloped in TiO_2 nanorod synthesised at 400 °C for 2 hrs

Fig. 8 shows the XPS scan for O 1s, three prominent peaks in the binding energy region of 530.6, 531.7 and 532.9 eV were found and correspond to Ti-O, O-C and C=O bond respectively. Out of these three peaks, the most dominant can be found in the binding energy region of 530.6 eV. The presence of this peak further support the formation of Ti-O bond of TiO_2, an indication of titanium atom bonded to oxygen. The XPS spectra further complements the EDS result shown in Fig. 3.

4. CONCLUSION

In this study, TiO_2 nanorods supported on stainless steel mesh was prepared via sol-gel methods followed by pyrolysis at different temperatures. Based on this investigation, the following conclusions were drawn. The HRSEM and HRTEM micrographs confirmed the formation of TiO_2 nanorods of different length at each synthesised temperature. The pyrolysis temperature influenced the phase, morphologies and the surface areas of the TiO_2 nanorods. The carbonaceous species obtained via the decomposition reaction of PVP in nitrogen atmosphere acts as dopant and adhesive respectively. The supported TiO_2 nanorods prepared by pyrolysis at 300 °C, 350 °C and 400 °C for 2 hrs was actually supported carbon doped TiO_2 nanocomposites. The average crystalline size of TiO_2 nanorod decreased from 45 nm to 28 nm as the temperature increases from 300°C to 400 °C at constant holding time of 2 hrs. Among all, the product obtained at 400 °C (2 hr) was found highly crystalline with highest porosity.

Acknowledgements

The authors acknowledge Dr. Franscious Cummings and Mr. Andrian Joseph of Physics Department, University of the Western Cape for the HRTEM and HRSEM analysis. Dr Remy Bucher (ithemba Labs, South Africa) who helped in XRD analysis. The authors are also grateful to Prof. Leslie Petrik, Environmental and Nanoscience Group, University of the Western Cape, South Africa for her insighful contribution to the manuscript.

REFERENCES

Álvarez, P.M., Jaramillo, J., López-Piñero, F., and Plucinski, P.K. (2010). Preparation and characterization of magnetic TiO2 nanoparticles and their utilization for the degradation of emerging pollutants in water. *Applied Catalysis B: Environmental*, 100: 338–345

Bestetti, M., Sacco, D., Brunella, M.F., Franz, S., Amadelli, R., and Samiolo, L. (2010). Photocatalytic degradation activity of titanium dioxide sol–gel coatings on stainless steel wire meshes. *Materials Chemistry and Physics*, 124: 1225–1231

Carrenõ, N.L.V., Garcia, I.T.S., Leidne S.S.M. Carrenõ, L.S.S.M., Nunes, M.R., Leite, E.R., Fajardo, H.V., and Probst, L.F.D. (2008). Synthesis of titania/carbon nanocomposites by polymeric precursor method. *Journal of Physics and Chemistry of Solids*, 69: 1897–1904

Chong, M.N., Jin, B., Chow, C.W.K., and Saint, C.P. (2010). Recent developments in photocatalytic water treatment technology: a review. *Water Resources*, 44: 2997–3027.

Gaya, U.I., and Abdullah, A.H. (2008). Heterogeneous photocatalytic degradation of organic contaminants over titanium dioxide: a review of fundamentals, progress and problems. *Journal of Photochemistry and Photobiology C*, 9(1): 1–12.

Gharakhlou, A.R. and Sarvi, M.N. (2017). Synthesis of mesoporous nanoparticles of TiO2 from ilmenite. *Materials Research Express*, 4, 025027

Hintsho, N., Petrik, L., Nechaev, A., Titinchi, S., Ndungu, P. (2014) Photo-catalytic activity of titanium dioxide carbon nanotube nano-composites modified with silver and palladium nanoparticles. *Applied Catalysis B Environment*, 156-157, 273

Jiang, Q., Li, L., Bi, J., Liang, S., and Liu, M. (2017). Design and Synthesis of TiO_2 Hollow Spheres with Spatially Separated Dual Cocatalysts for Efficient Photocatalytic Hydrogen Production. *Nanomaterials*, 7, 24-34

Kuriechen, S.K., and Murugesan, S. (2013). Carbon-Doped Titanium Dioxide Nanoparticles Mediated Photocatalytic Degradation of Azo Dyes Under Visible Light. *Water Air and Soil Pollution*, 224:1671-5

Lee, J.H., Kim, I.K., Cho, D., Youn, J.I., Kim, Y.J., Oh, H.J. (2015). Photocatalytic performance of graphene/Ag/TiO_2 hybrid nanocomposites. *Carbon Letter*, 16, 247- 257

Lia, Y., Guo, M., Zhang, M., and Wang, X. (2009). Hydrothermal synthesis and characterization of TiO_2 nanorod arrays on glass substrates. *Materials Research Bulletin*, 44(6): 1232–1237

Liu, X., Hong, H., Wu, X., Wu, Y., Ma, Y., Guan, W., Ye, Y. (2016). Synthesis of TiO_2–Reduced Graphene Oxide Nanocomposites for Efficient Adsorption and Photodegradation of Herbicides. *Water Air and Soil Pollution*, 227: 21

Mahendiran, R., Pandiyaraj, K.N., Kandavelu, V., and Saravanan, D. (2014). Investigation of Physico-Chemical Properties of TiO_2 Nanorod by Direct Sol Filling and Heating Sol-Gel Template Method. *Journal of Nanoscience and Nanotechnology*, 2(1): 79-82

Monreal, H.A, Chacon, N., Arce-Colunga, U., Martinez, C.A., Casillas, P.G., Martinez-Villafane, A. (2009). Sol–gel preparation of titanium dioxide nanoparticles in presence of a linear polysaccharide. *Micro and Nano Letters*, 4(4): 187-191

Nainani, R., Thakur, P., and Chaskar, M. (2012). Synthesis of Silver Doped TiO_2 Nanoparticles for the Improved Photocatalytic Degradation of Methyl Orange. *Journal of Materials Science and Engineering B*, 2 (1): 52-58

Nunes, D., Pimentel, A., Santos, L., Barquinha, P., Fortunato, E., and Martins, R. (2017). Photocatalytic TiO_2 Nanorod Spheres and Arrays Compatible with Flexible Applications. *Catalysts*, 7, 60

Omri, A., Benzina, M., and Bennour, F. (2015). Industrial application of photocatalysts prepared by hydrothermal and sol–gel methods. *Journal of Industrial and Engineering Chemistry*, 21: 356–362

Shinde, D.B., Jagadale, S.K., Mane, R.K., Mane, R.M., Ghanwat, V.B., Khot, K.V., Mali, S.S., Hong, C.K., and Bhosale, P.N. (2015). Time Dependent Facile Hydrothermal Synthesis of TiO_2 Nanorods and their Photoelectrochemical Applications. *Journal of Nanoscience and Nanotechnology*, S7:004. doi:10.4172/2157-7439.S7-00

Tijani, J.O., Fatoba, O.O., Totito, T.C., Roos, W.D., and Petrik, L.F. (2017). Synthesis and characterization of carbon doped TiO_2 photocatalysts supported on stainless steel mesh by sol-gel method. *Carbon Letter*, 22, 48-59

Wahyuningsih, S., Rinawati, L., Munifa, R.M.I, Ramelan, A.H., Sulistyono, E. (2017). TiO_2 Nanorods Preparation from Titanyl Sulphate Produced by Dissolution of Ilmenite. IOP Conf. Series: Materials Science and Engineering, 176, 012042

Zhao, J., Li, W., Li, X., and Zhang, X. (2017). Low temperature synthesis of water dispersible F-doped TiO_2 nanorods with enhanced photocatalytic activity. *Royal Society of Chemistry Advances*, 7, 21547–21555

Zhang, Z.L., Li, J.F., Wang, X.L., Qin, J.Q., Shi, W.J., Liu, Y.F., Gao, H.P., and Mao, Y.L. (2017). Enhancement of Perovskite Solar Cells Efficiency using N-Doped TiO_2 Nanorod Arrays as Electron Transfer Layer. *Nanoscale Research Letters*, 12, 43-50